NUCL SCI TECH (2018) 29:157
https://doi.org/10.1007/s41365-018-0489-7

Detailed study of RF properties of cold models for CW window-type RFQ

Qi Fu[1] · Kun Zhu[1] · Yuan-Rong Lu[1] · Zhi Wang[1] · Shu-Li Gao[1] · Fang-Jian Jia[1] · Yuan He[2]

Received: 7 December 2017 / Revised: 21 March 2018 / Accepted: 11 April 2018 / Published online: 27 September 2018

Abstract A 50 mA CW deuteron RFQ is being built for a joint 973 project between Peking University and the Institute of Modern Physics. This RFQ adopts a high-frequency window-type structure. To study its RF properties and to validate the reliability of an electromagnetic simulation, two full-length aluminum models with tuners were built in succession. RF measurements were obtained from the test bench and compared to the simulations, including frequencies, quality factors, and electric fields of different modes and the field in aperture. Through field tuning, the maximal field unflatness for a single quadrant and the average asymmetry of four quadrants were reduced from 8.7% and $\pm 3.6\%$ to 5.8% and $\pm 1.7\%$, respectively. Moreover, a tuning method of adjusting the gap distance between the endplates and the vanes was also studied in this paper.

Keywords CW RFQ · Cold model · RF measurement · Magnetic coupling window

This work was supported by the National Basic Research Program of China (No. 2014CB845503).

✉ Qi Fu
fuqi729@pku.edu.cn

Kun Zhu
zhukun@pku.edu.cn

Yuan-Rong Lu
yrlu@pku.edu.cn

1 State Key Laboratory of Nuclear Physics and Technology, Peking University, Beijing 100871, China

2 Institute of Modern Physics, China Academy of Science, Lanzhou 730000, China

1 Introduction

High-current continuous-wave (CW) RFQ is greatly needed for basic research [1–3], energy [4], medicine [5], etc., but this goal is filled with challenges. At present, the number of high-current CW RFQs that can operate stably is very limited around the world [6–10]. Therefore, PKU and IMP have been collaborating on a new 973 project that aims to build a 50 mA CW deuteron RFQ and challenge the difficulties in the beam dynamics, RF structure, cooling, and power coupling system. According to the beam dynamics design, this RFQ will operate at 162.5 MHz, accelerating a deuteron beam from 50 keV to 1 MeV with a length of 1.809 m [11]. In recent years, a new kind of four-vane RFQ with magnetic coupling windows, usually called a window-type RFQ, was developed by Argonne National Laboratory of America (ANL) and the Institution of Theoretical and Experimental Physics of Russia (ITEP) [12, 13]. It combines features of a four-vane RFQ and a four-rod RFQ, with the advantages of clear mode separation, compact structure, relatively low power consumption, and simple machining. To date, only a few low-frequency window-type RFQs for accelerating heavy ions worldwide have been built and commissioned. They have relatively small cross sections [14–17]. Thus, it is necessary to build and test cold models to lay a foundation for our power cavity.

2 First cold model experiment

The first cold model was built to study the effect of the magnetic coupling window's dimensions on the RF properties. As shown in Fig. 1, in the middle of each vane exists

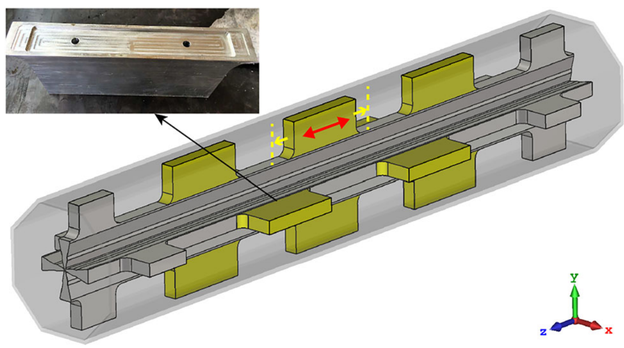

Fig. 1 Vanes of first cold model with wide windows and changeable blocks (Color online)

a very wide window. The supporting blocks, which are marked in yellow, can installed or detached at different locations with screws. By increasing the number of supporting blocks, the number of windows in each vane can be switched to three or four. Similarly, by changing the widths of the blocks, the window width can be changed to 220, 240 or 260 mm.

Figure 2 shows the resonant frequencies and mode separations (between the operating quadrupole mode and the nearest dipole mode) corresponding to three different values of window width. As can be seen, an increasing window width reduces the frequency and increases the mode separation. The results of the measurements are close to the data from simulations. In addition, the measured results of the three-window and four-window structures listed in Table 1 also agree with the simulated values. Note that to save on processing time and cost, the vanes of this cold model are not modulated, so the radius of the vane tip and the aperture are fixed. Their values are set to the maximum of the tip radius and the minimum of the aperture, respectively, according to the beam dynamics design.

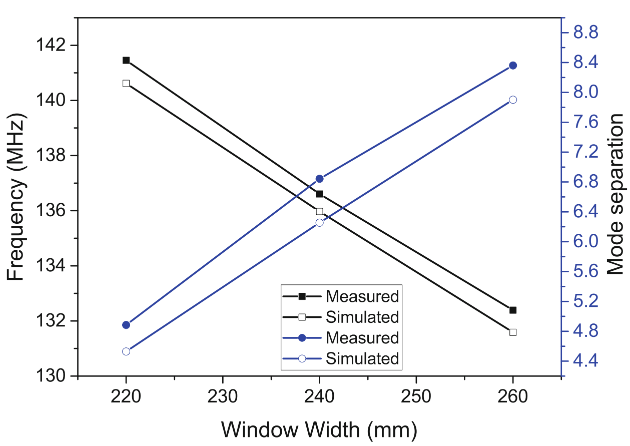

Fig. 2 Frequency and mode separation changes with window width (Color online)

Therefore, all of the measured frequencies are much lower than the designed values (162.5 MHz).

3 Second cold model experiment

The first model was useful in validating the relation of frequency and mode separation to the magnetic coupling windows. However, we noticed that cutting wide windows in the vanes impaired the mechanical strength of the aluminum structure, resulting in large deformations on the vane tips. Moreover, the cavity was assembled from many adjustable components, leading to poor electrical contact and very low quality factor of the cavity. Therefore, we built a second cold model with fixed-size windows. The detailed RF structure design of this cold model was presented in Ref. [18]. Its main parameters are summarized in Table 2. To leave a margin for tuning, the designed quadrupole mode frequency was a bit lower than the target value (162.5 MHz).

3.1 Fabrication

As shown in Fig. 3, the second RFQ cold model has three coupling windows in each vane and four 50-mm-diameter tuners equipped in each quadrant. To further improve electrical contact, the number of cavity walls was reduced from 16 to 8 (see Fig. 4), which is consistent with the power cavity.

Ball-end milling tools were employed when processing vane modulations, as the variable focusing strength in the beam dynamics design requires the transverse radius of the vane tip to change along the RFQ. Figure 5 shows a completed modulated vane. Finally, the eight parts were assembled in four steel frameworks for positioning.

3.2 RF measurement

The test bench to perform RF measurements on the cold model is shown in Fig. 6. It includes a two-port transmission network that consists of the RFQ cavity and two pickups, a network analyzer to measure the S-parameters, and a bead-pull system to sample the electric field in the cavity. Figure 7 shows the measurement of the resonant frequency and the loaded quality factor of the cold model, which are in the condition of very weak coupling and are based on an 3 dB method.

The conversion between the loaded and unloaded quality factors is given by

$$Q_0 = Q_L(1 + \beta_1 + \beta_2), \quad (1)$$

where β_1 and β_2 are the coupling coefficients of the two

Table 1 Comparison of simulated and measured frequencies with different numbers of windows in each vane

Number of windows	Frequency (MHz)		Mode separation (MHz)	
	Simulated	Measured	Simulated	Measured
3	135.971	136.606	6.255	6.843
4	131.379	132.195	7.130	8.236

Table 2 Design parameters of second RFQ cold model

Parameter	Value
Designed quadrupole mode (TE_{210}) (MHz)	161.979
Nearest dipole mode (TE_{110}) (MHz)	168.229
Nearest quadrupole mode (TE_{211}) (MHz)	180.206
Mode separation (MHz)	6.250
Window width (mm)	240.0
Window depth (mm)	80.0
Cavity radius (mm)	156.00
Minimum aperture radius (mm)	2.63
Vane tip radius (mm)	2.57–3.32
Length of RFQ vanes (m)	1.809
Quality factor	9808

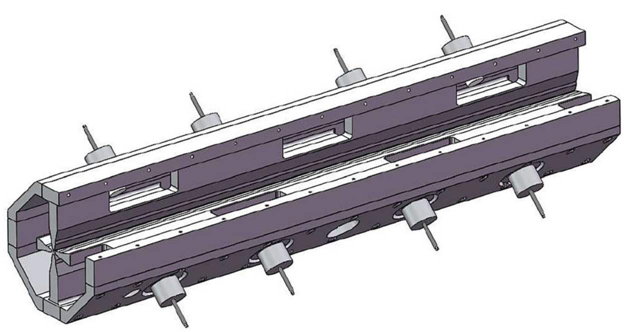

Fig. 3 Three-dimensional engineering model of second RFQ cold model (Color online)

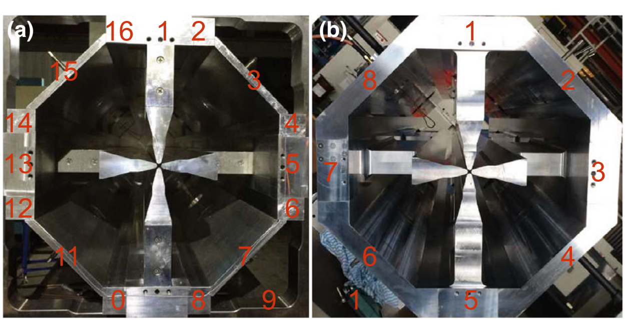

Fig. 4 Comparison of transverse views between **a** first model and **b** second model (Color online)

pickups. In our case, they are far less than 1 and are approximately equal. For this symmetrical coupling, the

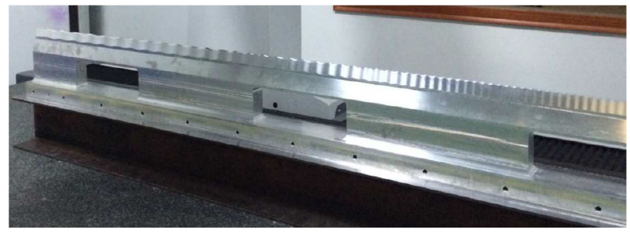

Fig. 5 One of the modulated vanes (Color online)

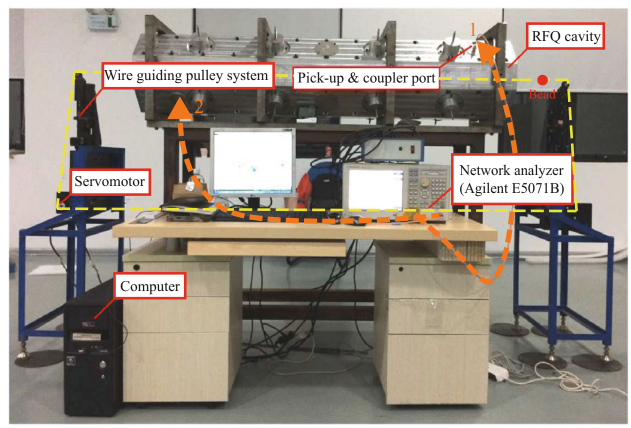

Fig. 6 Complete test bench (Color online)

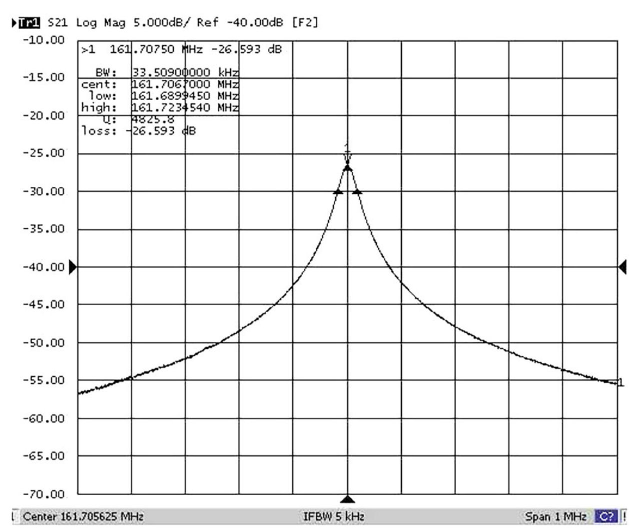

Fig. 7 Transmission coefficient (S_{21}) for operating mode

unloaded quality factor can also be calculated by substituting the measured S_{21} parameter into the following equation [19]:

$$Q_0 = \frac{Q_L}{1 - S_{21}}. \tag{2}$$

Table 3 lists the frequencies and unloaded quality factors we obtained for the first five modes. The measured unloaded quality factors are very close to the simulated values that were calculated with the electrical conductivity of aluminum ($\sigma = 1.9 \times 10^7\ \mathrm{sm^{-1}}$). The actual frequency of the operating mode is lower than that predicted by 0.272 MHz.

The classical bead-pull perturbation method was applied in the electric field measurement. When a small dielectric bead is displaced through the cavity, the resonant frequency shift $\Delta\omega$ and the electric field E at the bead's location satisfy the following relationship:

$$\frac{\Delta\omega}{\omega_0} = -\frac{3}{4}\frac{V_0}{W}\frac{\varepsilon_r - 1}{\varepsilon_r + 2}\varepsilon_0 E^2, \tag{3}$$

where V_0 is the bead volume and W is the stored energy of the cavity. In addition, the relationship between the frequency change and the phase change of the S_{21} parameter is

$$\tan\Delta\varphi = 2Q_L\frac{\Delta\omega}{\omega_0}. \tag{4}$$

As $\Delta\varphi$ is small ($\Delta\varphi < 10^o$), we have $\Delta\varphi \approx \tan\Delta\varphi$. Therefore, the electric field measurement acquires the square root of the phase shift $\Delta\varphi$.

We measured the field distribution of the first five modes in quadrant 1 at a distance of 15 mm from the aperture center. The phase shift caused by the network analyzer itself was already calibrated and corrected in raw data processing. As shown in Fig. 8, there is good agreement between the measured and simulated fields. The difference of the frequencies and field distributions between the two dipole modes ($^0TE_{110}$ and $^{\pi}TE_{110}$) confirms the asymmetric coupling windows between the horizontal and vertical

Table 3 Main parameters of second RFQ cold model

Mode	Simulated		Measured		
	f (MHz)	Q_0	f (MHz)	Q_0	S_{21}
TE_{210}	161.979	5614	161.707	5064	– 26.6
$^0TE_{110}$	168.229	6311	167.982	5573	– 28.2
TE_{211}	180.206	2730	180.438	2561	– 41.4
$^{\pi}TE_{110}$	181.635	3733	180.174	3210	– 33.5
$^0TE_{111}$	185.675	3042	185.958	3005	– 34.1

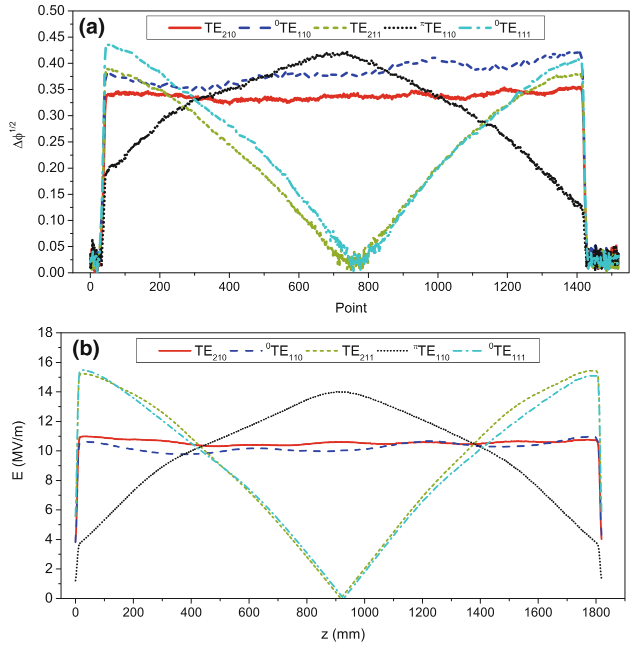

Fig. 8 **a** Measured and **b** simulated fields for first five modes (Color online)

vanes. The two figures also clearly show the noncoincidence of the zero points of the TE_{211} and $^0TE_{111}$ modes owing to their different frequencies.

In addition, we measured the field in aperture by guiding a 4-mm-diameter bead along the axis. Owing to the nonzero volume of the bead, the obtained field was actually the average field inside the bead. Thus, a 1-mm-off-axis field calculated with CST EM [20] was used for comparison. As shown in Fig. 9, these two field distribution curves are highly consistent with each other, which confirms the accuracy of the vane modulation of the cold model.

3.3 Tuning

Tuners equipped in the RFQ cavity can change the cavity volume and compensate for the impact of machining and assembly errors and material deformation, thereby

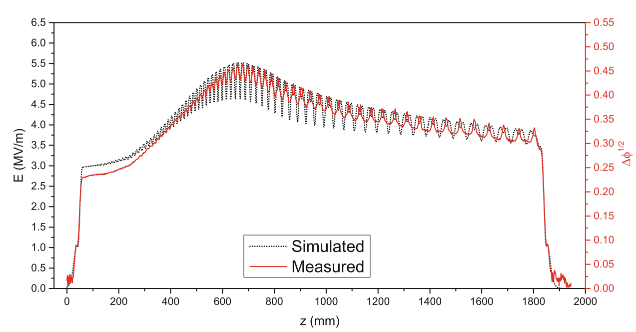

Fig. 9 Comparison of simulated and measured fields in aperture (Color online)

tuning both the frequency and field distribution to achieve the design requirements. Owing to the nonuniform magnetic field distribution caused by the coupling windows, there are small differences in tuning capability between the tuners in different longitudinal positions. When all 16 tuners are inserted the same distance into the cavity, the change in the frequency and quality factor for the first mode with distance is shown in Fig. 10. The tuning range of the frequency is approximately 0.9 MHz, and the average tuning sensitivity is 1.11 kHz mm^{-1} for one tuner.

Before field tuning, we measured the electric field distribution in the four quadrants (see Fig. 11). To analyze the field unflatness, the measured fields were normalized by dividing them by their average value, as shown in Fig. 12a. The black curve is the average field of the four quadrants. Owing to unavoidable material deformation and assembly errors, quadrant 3 has a large deviation compared with the other three quadrants, and the maximal field unflatness for a single quadrant reaches 8.7%. In addition, we notice that the field distribution in the four quadrants is correlated with the distances between adjacent vanes at the entrance and exit (see Table 4). For instance, $D4$ is much shorter than the other three distances at the entrance, and thus, the field in quadrant 4 has the highest field. Similarly, $D1$ is shorter than $D2$ at the exit, so the field in quadrant 1 is higher than that in quadrant 2.

Then, we analyzed the asymmetry of each quadrant field, which can be calculated by the following equation:

$$\text{Asymmetry} = \frac{E_{\mathrm{Qk}} - \overline{E_{\mathrm{k}}}}{\overline{E_{\mathrm{k}}}} \times 100\%, \tag{5}$$

where E_{Qk} is the measured field at longitudinal position k in quadrant Q and $\overline{E_{\mathrm{k}}}$ is the average field of the four quadrants at k. From Fig. 11, one can see that the influence of gravity on the guiding wire means that the bead is closer to the horizontal vanes in quadrants 1 and 2, whereas it is the opposite in quadrants 3 and 4. Thus, the field

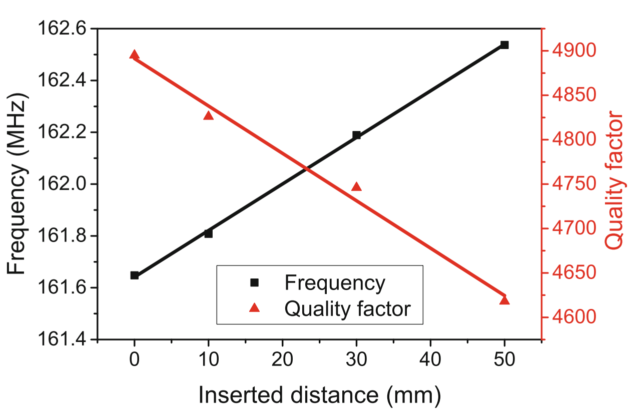

Fig. 10 Change in first-mode frequency and quality factor with inserted distance of tuners (Color online)

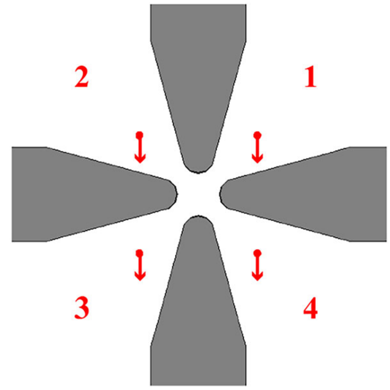

Fig. 11 Influence of gravity on electric field measurement

distribution curves for quadrants 1 and 2 bend upward, whereas those for quadrants 3 and 4 bend downward, as shown in Fig. 12c. To eliminate this influence, we averaged the asymmetries between quadrants 1 and 4 and between quadrants 2 and 3, and plotted them as black and blue curves, respectively. These indicate an obvious asymmetry in the horizontal direction of the cavity, which is $\pm 3.6\%$ on average.

After adjusting the inserted distance for each tuner, the fields and asymmetries of the four quadrants are shown in Fig. 12b, d, respectively. Although the average unflatness changed little, the maximal unflatness is down to 5.8% and the average asymmetry is also reduced by half. However, we noticed that to obtain these relatively flat fields, several tuners were inserted at the deepest distance, yet the operating mode frequency was only 162.140 MHz. This indicates that the tuning capability is inadequate for this cold model. Therefore, the number of tuners in each quadrant will be increased from 4 to 7 and the tuner diameter will also be enlarged from 50 to 60 mm for the copper power cavity, thereby increasing the tuning range of the frequency to 2.5 MHz.

3.4 Gap tuning

As the vertical vanes have no coupling windows at either end (see Figs. 3 or 4) and are very close to the endplates, the operating mode frequency and the distribution trend of the electric field are quite sensitive to the gaps between the endplates and the vanes, just as end cuts for a four-vane RFQ. By adding shims between the endplate and the cavity, we increased the gap distance at the entrance from 8 mm to 11 and 14 mm. As shown in Fig. 13, increasing the gap distance at the entrance can correct the slant field and increase the operating mode frequency in a nonlinear fashion. This changing effect can be used as an alternative method for tuning our power cavity.

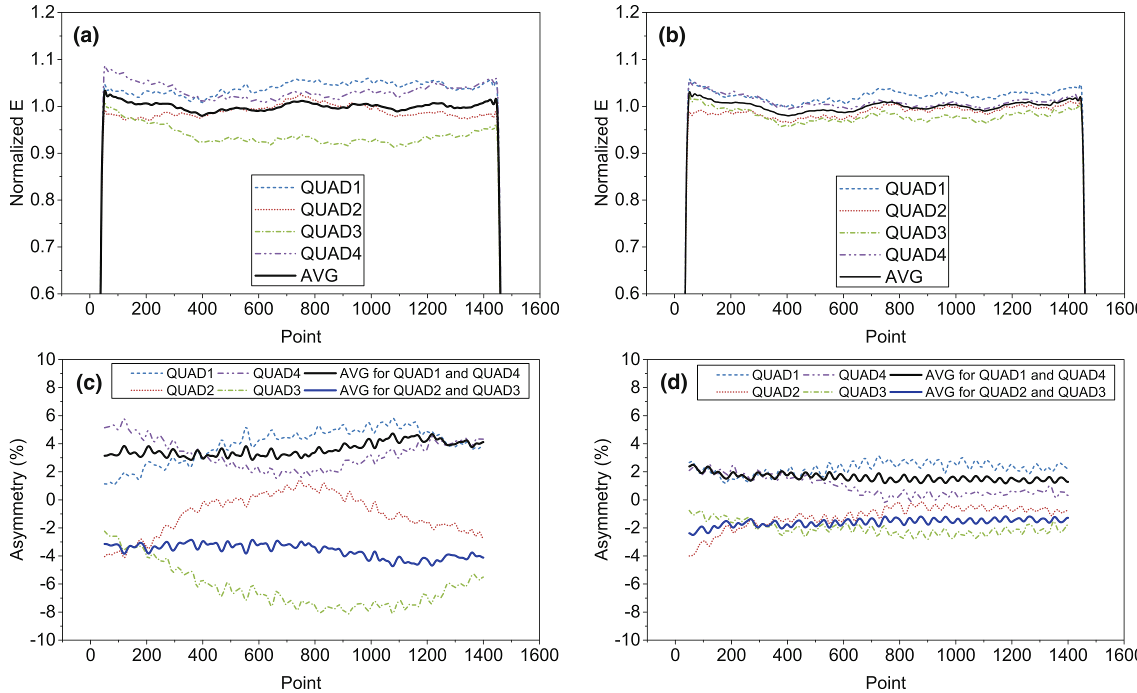

Fig. 12 Normalized fields in four quadrants **a** before and **b** after tuning, and asymmetries of four quadrants **c** before and **d** after tuning

Table 4 Dimension parameters of the second RFQ cold model

Quadrant	Entrance		Exit	
	Measured distance (mm)	Simulated distance (mm)	Measured distance (mm)	Simulated distance (mm)
*D*1	4.01	3.98	4.29	4.31
*D*2	4.02	3.98	4.38	4.31
*D*3	4.01	3.98	4.33	4.31
*D*4	3.91	3.98	4.33	4.31

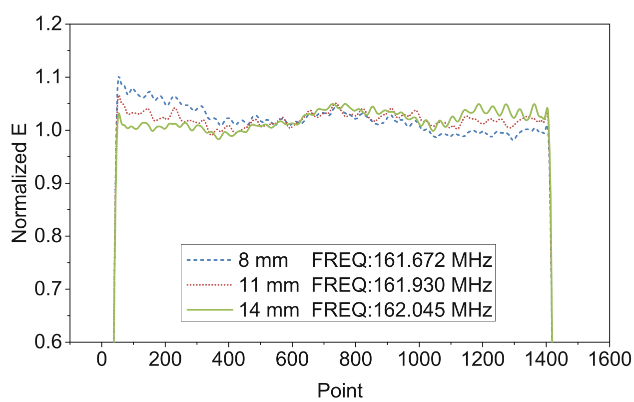

Fig. 13 Effect of distance changes in gap between entrance endplate and vanes on field in quadrant 4 and frequency of operating mode (Color online)

4 Conclusion

We built and studied two aluminum cold models of a window-type RFQ. By measuring the first model with variable coupling windows, we verified the relationship frequency and mode separation with the dimension and number of the windows. For the second model, we measured the frequencies, quality factors, and electric fields of the first five modes and the field in aperture based on the test bench. The results agree well with the simulated results, thereby confirming the reliability of the simulations. In addition, we carried out an analysis on the unflatness and asymmetry of each quadrant field and tuned the field using 16 tuners. With limited tuning capability, we obtained relatively flat fields. Finally, we measured the effect of changes in the gap distance on the field distribution and the operating mode frequency. This work provided significant experience for the manufacture and measurement of a power cavity. Now, this cavity is being processed in a factory in Lanzhou. RF measurement and high-power tests will be performed later in 2018.

References

1. A. Pisent, in *Proceedings of the 25th Linear Accelerator Conference*, Tsukuba, Japan, 12–17 September (2010), pp. 372–376
2. J. Galambos, in *Proceedings of North American Particle Accelerator Conference*, Pasadena, CA USA, 29 September–4 October (2013), pp. 1443–1447
3. H.F. Ouyang, S.N. Fu, in *Proceedings of the 23rd Linear Accelerator Conference*, Knoxville, Tennessee USA, 21–25 August (2006), pp. 746–748
4. Z.L. Zhang et al., in *Proceedings of the 26th Linear Accelerator Conference*, Tel-Aviv, Israel, 9–14 September (2012), pp. 942–944
5. J. Guzek, U. Tapper, W. McMurray, J.I. Watterson, Characterization of the 9Be (d, n) 10B reaction as a source of neutrons employing commercially available radio frequency quadrupole (RFQ) linacs, in *Proceedings of SPIE, International Conference Neutrons in Research and Industry*, vol. 2867 (1997). https://doi.org/10.1117/12.267963
6. A. Patrick et al., in *Proceedings of the 5th International Beam Instrumentation Conference*, Barcelona, Spain, (2016), pp. 413–416
7. E. Fagotti, L. Antoniazzi, A. Palmieri, F. Grespan, in *Proceedings of the 26th Linear Accelerator Conference*, Tel-Aviv, Israel, 9–14 September (2012), pp. 828–830
8. A. Pisent, in *Proceedings of the 28th Linear Accelerator Conference*, East Lansing, MI, USA, 25–30 September (2016), pp. 698–703
9. A. Kreisel et al., in *Proceedings of the 27th Linear Accelerator Conference*, Geneva, Switzerland, 31 August–5 September (2014), pp. 770–774
10. R. Ferdinand, P.E. Bernaudin, P. Bertrand et al., in *Proceedings of the 8th International Particle Accelerator Conference*, Copenhagen, Denmark, 14–19 May (2017), pp. 2462–2465
11. F.J. Jia, K. Zhu, Y.R. Lu, Z. Wang, Z.Y. Guo, Q. Fu, Y. He, Beam dynamics design of a 50 mA D+ RFQ. Chin. Phys. Lett. **33**(7), 072901 (2016). https://doi.org/10.1088/0256-307X/33/7/072901
12. P.N. Ostroumov, A.A. Kolomiets, D.A. Kashinsky, S.A. Minaev, V.I. Pershin, T.E. Tretyakova, S.G. Yaramishev, Design of 57.5 MHz cw RFQ for medium energy heavy ion superconducting linac. Phys. Rev. ST Accel. Beams **5**(6), 060101 (2002). https://doi.org/10.1103/PhysRevSTAB.5.060101
13. V. Andreev, G. Parisi, in *Proceedings of the 15th Particle Accelerator Conference*, Washington, DC (1993), pp. 3124–3126
14. V. Andreev, N.N. Alexeev, A. Kolomiets, V. Koshelev, B. Kondratyev, A. Kozodaev, V. Kuzmichev, Y. Orlov, V. Stolbunov, T. Tretyakova, in *Proceedings of the 2nd International Particle Accelerator Conference*, San Sebastián, Spain, 4–9 September (2011), pp. 2622–2624
15. P.N. Ostroumov, B. Mustapha, A. Barcikowski, C. Dickerson, A.A. Kolomiets, S.A. Kondrashev, Y. Luo, D. Paskvan, A. Perry, D. Schrage, S.I. Sharamentov, R. Sommer, W. Toter, G. Zinkann, Development and beam test of a continuous wave radio frequency quadrupole accelerator. Phys. Rev. ST Accel. Beams **16**(11), 110101 (2012). https://doi.org/10.1103/PhysRevSTAB.15.110101
16. A. Perry, C. Dickerson, P.N. Ostroumov, G. Zinkann, Beam characterization of a new continuous wave radio frequency quadrupole accelerator. Nucl. Instrum. Methods Phys. Res. Sect. A **735**, 163–168 (2014). https://doi.org/10.1016/j.nima.2013.08.002
17. V. Koshelev, G. Kropachev, T. Kulevoy, D. Liakin, A. Plastun, S. Vinogradov, S. Polozov, A. Butenko, in *Proceedings of the 28th Linear Accelerator Conference*, East-lansing, MI, 25–30 September (2016), pp. 575–577
18. Q. Fu, P. Gan, S. Gao, F. Jia, H. Li, Y. Lu, Z. Wang, K. Zhu, J. Liu, in *Proceedings of the 7th International Particle Accelerator Conference*, Busan, Korea, 8–13 May (2016), pp. 423–425
19. D. Kajfez, *Q Factor Measurements, Analog and Digital* (Department of Electrical Engineering, University of Mississippi, Oxford, 1999)
20. CST, http://www.CST.com. Accessed 7 Dec 2017